Nanoscale

Accepted Manuscript

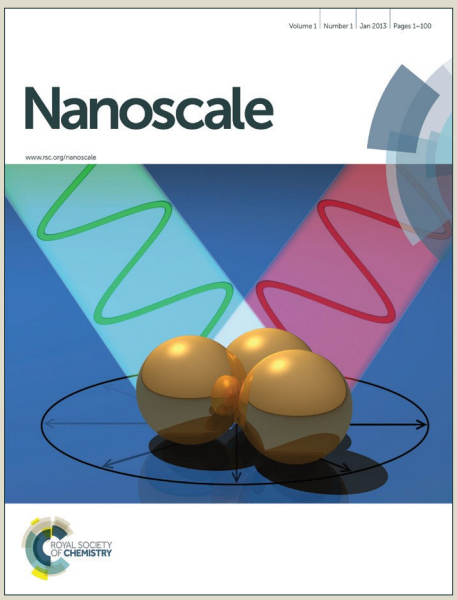

ROYAL SOCIETY OF CHEMISTRY

www.rsc.org/nanoscale

Nanoscale

ARTICLE

In-situ Degradation Studies of Two-dimensional WSe_2-Graphene Heterostructures

Received 00th January 20xx,
Accepted 00th January 20xx

DOI: 10.1039/x0xx00000x

www.rsc.org/

B. Wang [a,b], S. M. Eichfield[b,c], D. Wang,[b,c] J. A. Robinson[b,c] and M. A. Haque[a,b]

Heterostructures of two-dimensional materials can be vulnerable to thermal degradation due to structural and interfacial defects as well as thermal expansion mismatch, yet a systematic study is yet to exist in the literature. In this study, we investigate the degradation of freestanding WSe_2-graphene heterostructures due to heat and charge flow by performing insitu experiments inside the transmission electron microscope. Experimental results show that purely thermal loading requires higher temperatures (>850 °C), about 150 °C higher than that under combined electrical and thermal loading. In both cases, selenium is the first element to decompose and migration of silicon atoms from the test structure to the freestanding specimen initiate rapid degradation through the formation of tungsten disilicide and silicon carbide formation. The role of current flow is to enhance the migration of silicon from the sample holder and to knock-out the selenium atoms. The findings of this study add fundamental insights to the degradation of WSe_2-graphene heterostructures and inspire their application in harsh environment electronics.

Received 00th January 20xx,
Accepted 00th January 20xx

DOI: 10.1039/x0xx00000x

www.rsc.org/

Introduction

Two-dimensional materials and their heterostructures have received tremendous attention for unusual physical phenomena and promise in opto/electronics, energy conversion, physical and bio sensing as well as bulk composite applications[1]. Their layered structure, with strong in-plane covalent or ionic and weak cross-plane van der Waals bonding, enables stability in mono to few-layer form. The predominance of surface atoms without the deleterious dangling bond defects results in unprecedented charge and heat transport confined to a plane[2]. This allows aggressive transistor channel length scaling without compromising the materials intrinsic properties. Starting with graphene, the literature has seen explosive growth in these phenomena and applications, especially after materials with complementary characteristics. For example, electrically insulating yet thermally conducting hexagonal boron nitride[3] and semiconducting 2D transition metal dichalcogenides (TMD), such as MoS_2 and WSe_2 [4] have catalysed the concept and realization of heterostructures [5]. In comparison, structural stability of these atomic layered structures have received less attention. In particular, very little is known about their thermal stability or degradation mechanisms, probably because their high temperature compatibility. Nevertheless, the predominance of surface atoms also makes 2D materials susceptible structural and topological defects as well as external stimuli. This is the core theme of this study, where we investigate the effects of heat and charge flow on the degradation of 2D WSe_2-graphene structure. The experiments are performed in-situ inside a transmission electron microscope (TEM) after integrating the specimens with micro-electro-mechanical devices for thermal and electrical loading.

Compared to graphene, TMDs are more attractive because of their electronic structure and its tunability that gives to rise the valley polarization, which lends to device physics in addition to charge and spin[6]. Quantum confinement effect alters the electronic structures in monolayer TMDs from an indirect to direct bandgap,[7, 8] enhancing light-matter-charge interactions as well as electrochemical reactivity.[9] Even though MoS_2 has been popular in the literature, we focus on the emerging 2D version of WSe_2. It possesses mechanical flexibility, optical transparency and direct band gap of 1.65 eV, making monolayer WSe_2 attractive for electronic and optoelectronic devices.[10, 11] It is composed of two-dimensional trilayer Se–W–Se structures, with a W atom plane in the middle of two hexagonal Se atom planes. It is also the first TMD material combining p-type and n-type characteristics (depending on the metal contact used),[12, 13] offering the possibility of complementary logic circuits in the same monolayer. Exfoliated monolayer WSe_2-based transistors show impressive carrier mobility[14, 15] (up to 650 $cm^2\ V^{-1}\ s^{-1}$) with >10^6 on/off ratio[16].

In this study, we focus on the structural stability and degradation of 2D heterostructure of WSe_2 on graphene, which is critical for device performance and reliability. Our motivation comes from the striking lack of research in this area involving 2D materials and their heterostructures. Limited studies on thermal degradation of graphene[17, 18] and layer by layer thinning of MoS_2[19] indicate the influence of temperature. The reason could be the known electro-chemical and thermal stability of commonly studied 2D materials, such as graphene[20]. However, this may not necessarily true for

[a] Mechanical & Nuclear Engineering, 314 Leonhard Building, the Pennsylvania State University, PA 16802, USA. Email: mah37@psu.edu
[b] Center for Two-Dimensional and Layered Materials, Millennium Science Complex, The Pennsylvania State University, PA 16802, USA.
[c] Materials Science and Engineering, The Pennsylvania State University, PA 16802, USA. Email: jrobinson@psu.edu

† Footnotes relating to the title and/or authors should appear here.
Electronic Supplementary Information (ESI) available: [details of any supplementary information available should be included here]. See DOI: 10.1039/x0xx00000x

Please do not adjust margins

emerging materials.[21] Even for chemically and thermal stable components, their heterostructures can be vulnerable to degradation due to structural and interfacial defects, especially at higher temperatures and/or electrical current densities. Thermal expansion mismatch can have strong influence since their negative thermal expansion coefficients imply tensile strain at higher temperatures. To the best of our knowledge, no study exists in the literature on degradation of either WSe_2 or any related heterostructures. Similar shortcoming for most other 2D materials in the literature highlights the significance of this research. We also note that synthesis of 2D WSe_2[22], in particular heterostructures[23, 24], remains challenging and emerging area of research in the literature.

Experimental

The experimental setup consists of a freestanding WSe_2-graphene heterostructure integrated with a micro-electro-mechanical device with a micro-actuator and a micro heater. Figure 1a shows the entire setup, where the 5mm x 3 mm size device is mounted on an electrical biasing TEM specimen holder. The test chip was fabricated on a heavily doped silicon-on-insulator wafer with 20 micron thick device layer. After photolithographic patterning, deep reactive ion etching was used to realize the device structure. A second lithography with backside alignment was performed on the handle layer, followed by a through-the-thickness deep reactive ion etching. The buried oxide was removed by vapour phase hydro-fluoric acid etch to make the device freely suspended. This allows imaging and diffraction of any electron transparent specimen inside the TEM. Figure 1b shows scanning electron micrograph of the device after wire-bonded to the TEM specimen holder. It also shows two sets of electrodes, PQ and RS, to power up the heaters and thermal actuators respectively. Even though they both operate on Joule heating, their different geometry leads to different specimen configuration upon electrical biasing. Figure 1c shows the heaters. When transferred on to it, 2D materials would form rectangular bridges along the direction of the current flow as shown in Figure 1c. When the PQ electrodes are electrically biased, the current will pass through both the silicon heater and the freestanding specimen. Therefore, the specimen experiences both thermal and electrical loading. Figure 1e illustrates the different nature of specimen transfer in the actuator area, where the suspended specimens are aligned perpendicular to the direction of electrical biasing (electrodes RS). This results in pure thermal loading of the specimen.

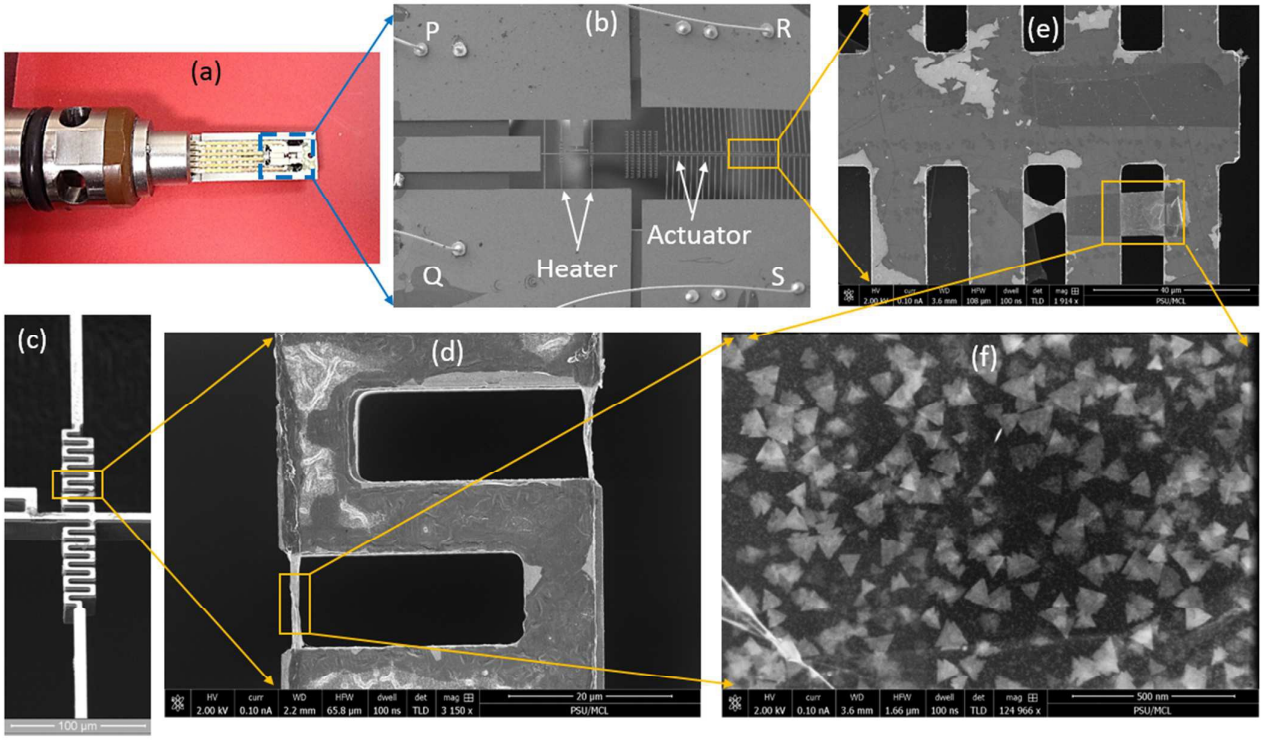

Fig. 1 (a) experimental consisting of a micro-electro-mechanical devices mounted on an electrical biasing TEM holder (b) zoomed view of the device showing heater and actuator areas (c) zoomed view of a heater (d) zoomed view of a freestanding WSe_2-graphene heterostructure on the heater area (e) zoomed view of a freestanding specimen in the actuator area (f) triangle shaped domains of highly crystalline WSe_2 on graphene.

While most of the monolayer WSe_2 is commonly obtained from mechanical exfoliation,[14, 25, 26] we directly chemical vapour deposited (CVD) the WSe_2 on freestanding bilayer graphene already laid out on the micro device. CVD growth of WSe_2 is only emerging in the literature[11, 22] and is better suited towards building heterostructures[5, 15] on graphene compared to other vapour transport,[27, 28] or transition metal selenization[13, 29] processes. Graphene films are grown via chemical vapor deposition on copper substrates[30], and subsequently transferred to the fabricated TEM test structures (Fig 1a-d). Subsequently, samples were loaded into a metal-organic chemical vapour deposition system, where WSe_2 domains were synthesized from tungsten hexacarbonyl ($W(CO)_6$)

and dimethylselenide ($(CH_3)_2Se$) on the suspended graphene layers at 800°C and 700 Torr using Se/W ratio of 14000[22, 23] (Fig. 1f). All the experiments in this study were performed at 80 kV acceleration voltage in a JEOL 2010 TEM. Signs of electron beam induced damage was rigorously monitored in the specimen.

Results and discussion

In-situ TEM experiments were performed to visualize the degradation of WSe_2-graphene heterostructure under purely thermal as well as thermo-electrical loading. To estimate the temperature of the micromachined heaters as function of the supplied current, an infrared microscope was used to measure the real temperature of a similar device at 20 milli-Torr vacuum. The experimental data is then used to calibrate a finite element model that simulates the device temperature. The model accounts for the radiation losses that dominates over convection at these vacuum levels. The technique is then validated by melting thin films of pure metals with known melting points. Details of the temperature estimation technique is given elsewhere.[31]

Temperature Effects

As shown in Figure 1, the position and orientation of the 2D heterostructure can be exploited to control the flow of heat and charge in it. Figure 2 shows TEM images and diffraction patterns after passing current through the thermal actuator (Figure 1e). The discrete spots in the diffraction pattern come from two layers of graphene, while the ring patterns come from the smaller WSe2 domains. In this specimen configuration, there is no current flow in the specimen and the degradation effects are due to temperature only. The specimen temperature was incremented by 20 °C after 700 °C with hold times of 30 minutes between each increments. The specimen showed remarkable thermal stability up to about 800°C, since almost no change in microstructure or diffraction pattern was observed. . Figure 2a shows the specimen at 820°C when the sharp edges of the triangular WSe_2 domains start to lose sharpness. This is quite expected since the edges of the domains possess higher energy, they are the first ones to show instability. The degradation process was very rapid at this phase since WSe_2 started to melt at 860°C. This matches well with the decomposition temperature of bulk WSe_2 in vacuum[23]. The diffraction pattern at this temperature suggests that graphene maintains its integrity. It also suggests presence of silicon carbide in the specimen. The observation of degradation at temperature similar to deposition indicates stability of the heterostructure under high vacuum condition inside the TEM. In comparison, the deposition was performed at 700 Torr pressure. At only 880°C, graphene also becomes unstable and undergoes a phase change reflected by very strong change in contrast in the bright field mode. The multitudes of diffused rings in the corresponding diffraction patterns suggests that the single crystal degraded to nanocrystalline domains of many different alloys or elements. We indexed these rings to identify the constituents and found no trace of pure tungsten or selenium. The pattern matched very well with silicon carbide. However, there were other rings that could not be unambiguously indexed, suggesting other alloys than pure tungsten or selenium.

To understand the basic mechanisms behind thermal degradation, we performed both energy dispersive (EDS) and Raman spectroscopy on the specimen. A WITec confocal Raman system with a 488nm excitation wavelength was used this study. These results are shown in Figure 3. Very strong presence of silicon was observed which is interesting since the freestanding specimen was supported at the ends by the micromachined silicon structures. The growth and transfer process are least likely to contaminate with silicon. The gradient in the silicon profile (Figure 3a) indicates the migration of silicon from the test device structures to the freestanding WSe_2-graphene surface. This atomic scale mass transfer takes place due to surface diffusion. Density functional theory (DFT) suggests the diffusion barrier for silicon on graphene can be as small as 0.06 eV, and van der Waals interaction between silicon adatom and graphene sheet has only a minimal effect on the diffusion barrier[3]. While high mobility of silicon adatoms on graphene can explain the presence of silicon in our specimen, the Raman peak at 520 cm^{-1} is most likely from the micromachined silicon structures. The Raman spectra confirms the other alloys originating from silicon, carbon and tungsten. For example the 330 and 450 cm^{-1} peaks indicate presence of due to tungsten disilicide[3]. Tungsten disilicide can nucleate at as low as 500 °C with ultra-fine grains that increase up to 160 nm at 800 °C[6]. Another alloy present was silicon carbide (SiC). The 800 cm^{-1} peak is the signature of 3C-SiC while the 900 band is for amorphous SiC [4]. Thermal degradation of the graphene is reflected by the G-band at about 1580 cm^{-1} showing the in-plane displacement of carbon atoms in the hexagonal sheets. The band at about 1350 cm^{-1} (D-band) is due to the disorder of the structure.

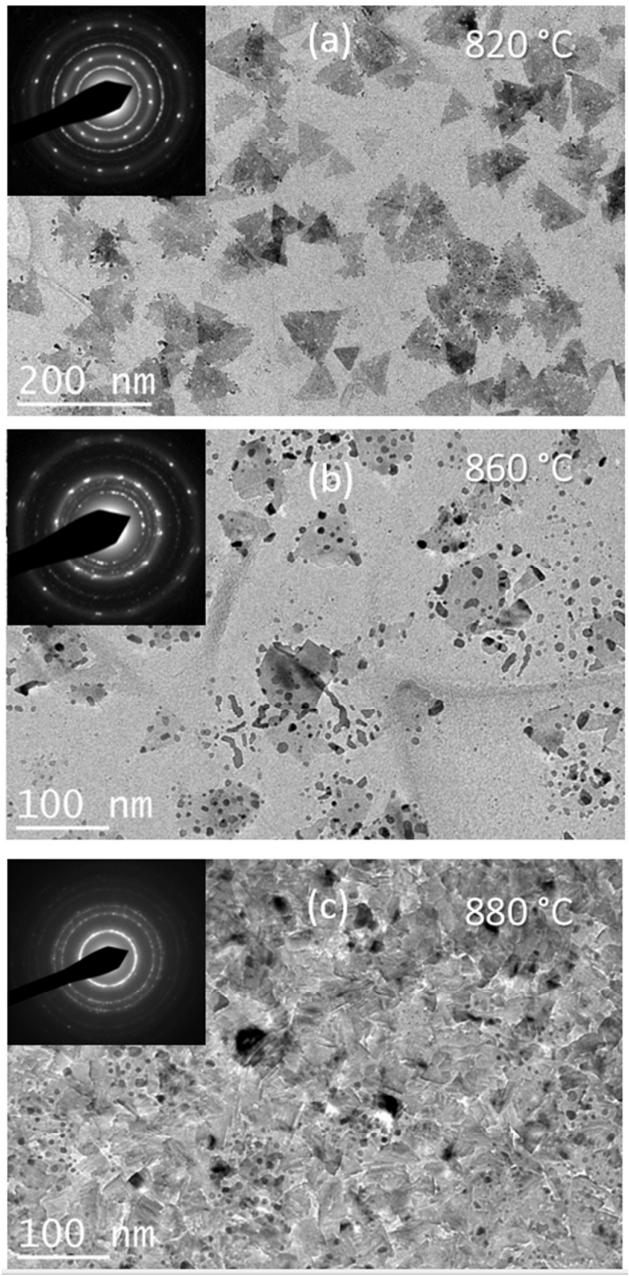

Fig. 2 In-situ TEM observation of the microstructure and corresponding electron diffraction patterns at various temperatures.

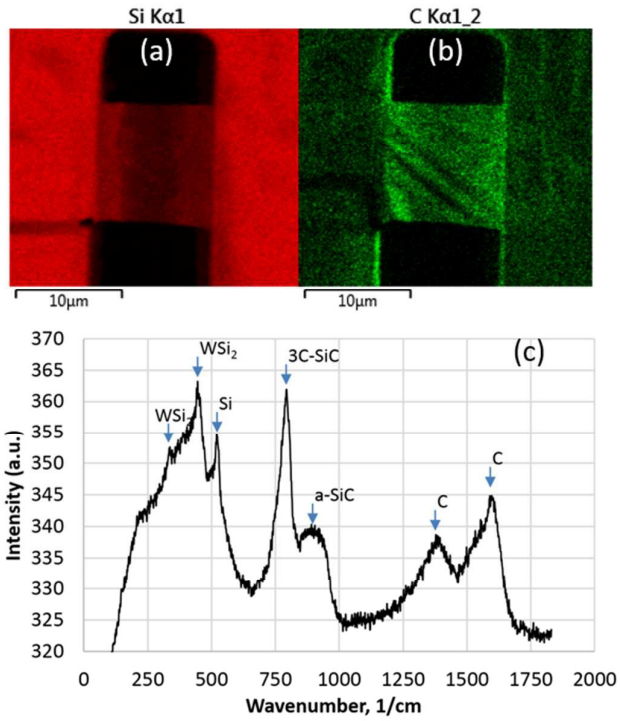

Fig. 3 Energy dispersive spectroscopy of the thermally degraded WSe_2-graphene heterostructure showing (a) surface diffusion of silicon and (b) carbon (c) Raman spectra suggesting various alloys of tungsten, silicon and carbon

Current and Temperature Effects

The serpentine silicon heater structure (Figures 1c and 1d) induces a temperature field, which is uniform given the small size of the specimen. Since the specimen is electrically parallel to the heater and along the electrical biasing direction, it also experiences current flow. For such a parallel current flow, the current density in the specimen can be obtained from the respective resistances of the specimen and silicon structures. The resistance of the 10 micron wide, 10 micron long and 20 micron thick silicon beam is approximately 1 ohm after we measured its resistivity to be 0.002 ohm·cm. Similarly, resistance of the 2.7 micron wide, 10 micron long and 0.345 nm thick graphene specimen can be estimated to be 4625 ohms after measuring the resistivity to be $4.31e^{-5}$ ohm·cm. The current density in the specimen can be estimated from these figures after passing a known current in the heater.

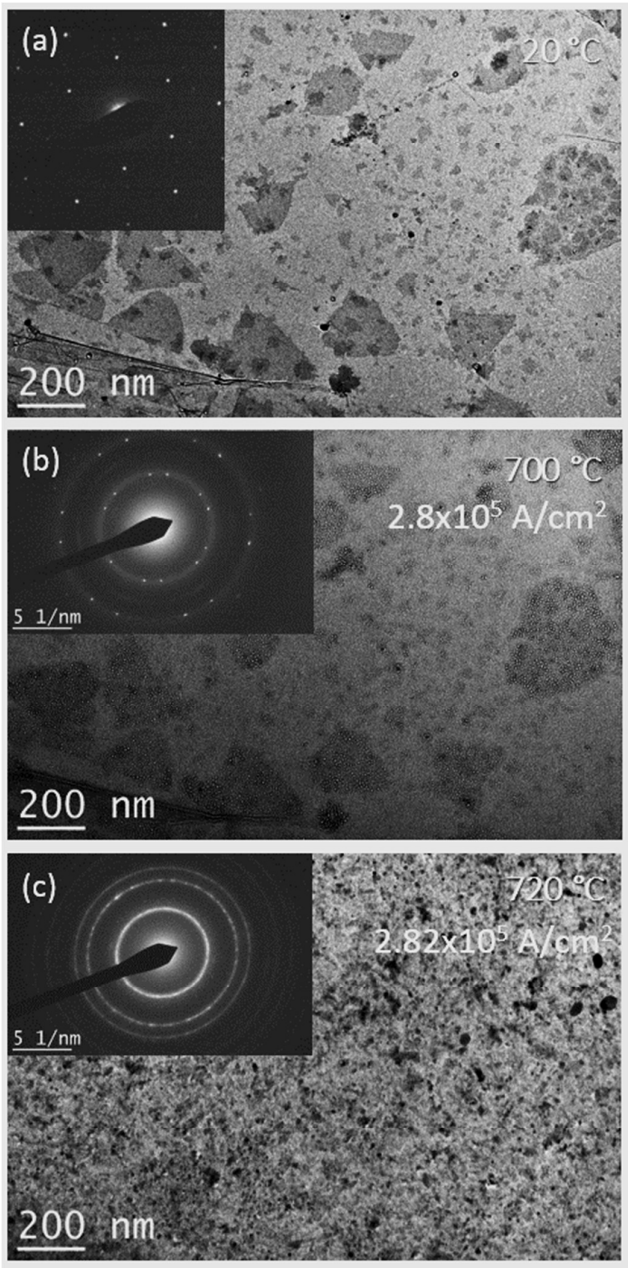

Fig. 4 Energy dispersive spectroscopy of the thermally degraded WSe_2-graphene heterostructure showing (a) surface diffusion of silicon and (b) carbon (c) Raman spectra suggesting various alloys of tungsten, silicon and carbon

A remarkable difference in degradation temperature and mechanism was observed (Figure 4) when passing current through the heater section (Figure 1c). At about 700 °C, the WSe_2 domains appear to blister and the corresponding TEM diffraction pattern shows tungsten only, suggesting the decomposition of selenium. We propose that the effect of the current density (about $2.8x10^5$ A/cm^2) in the specimen is to facilitate the knockout of the selenium atoms due to the momentum transfer of the electrons. At higher current density, the electron wind can promote transfer of silicon atom contaminants from the silicon heater to the graphene-WSe2 heterostructure through phenomena similar to electro and thermo migration[9, 32, 33] . The role of silicon contamination is to create alloying effects after reacting with highly crystalline graphene. These alloys create nanocrystalline grains, thereby catastrophically degrading the specimen. In other words, the electron wind catalyses the decomposition, thereby lowering the temperature. We suggest that the influences of temperature and current are synergistic because the presence of current density results in the initiation of degradation at about 160 °C lower than thermal only decomposition. At about 720 °C, there is a very sharp contrast change in the specimen, after which the microstructure and diffraction pattern essentially appear to be similar to thermal degradation (Figure 2c) alone.

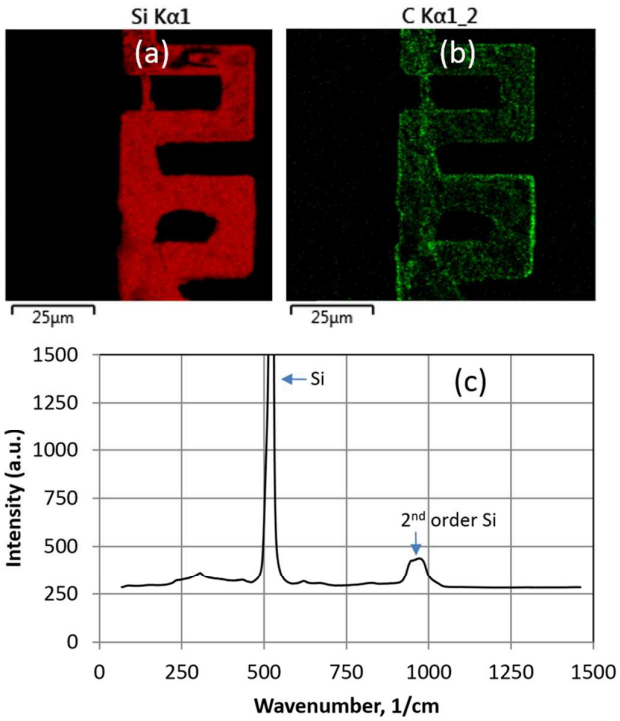

Fig. 5 Energy dispersive spectroscopy of the electro-thermally degraded WSe_2-graphene heterostructure showing (a) surface diffusion of silicon and (b) carbon (c) Raman spectra suggesting alloying of silicon carbide and tungsten disilicide.

Energy dispersive spectroscopy in Figures 5a and 5b clearly show the presence of silicon, tungsten (overlaps with silicon) and carbon in the degraded specimen. The Raman spectroscopy in Figure 5c however shows predominance of silicon only. The wide (940 cm^{-1} to 990 cm^{-1}) peak can be related to the second-order transversal optical phonons as observed in bulk crystalline silicon.[34] SiC crystallites also show a wide peak at this wavenumber[35], but in that case, a first order peak would also have been present at 790 cm^{-1} This conflicts with the finding in Figure 5b, because carbon in form of alloys or allotropes must be present in the specimen. To resolve this, we examine the TEM diffraction patterns in Figures 2 and 4, where they were not indexed for legibility. The results are shown in Figure 6, where expected diffraction patterns for both Si and SiC are superimposed. Clearly, SiC is a better match, comparing the first two rings. We propose that both Si and SiC are present depending on the availability of Si through surface migration, which is not captured in the Raman spectra because it collects information from the specimen surface only. The migrated Si reacts with the carbon from degraded graphene to form SiC. At some point, all the carbon becomes depleted through this process. This is supported by the absence of carbon peaks, compared to purely thermal loading (Figure 3c). After this, Si continue to migrate over the SiC layer. Since TEM is a through the thickness technique, it shows both Si and SiC, whereas Raman spectroscopy shows the surface elements only. The depletion of carbon in Figure 5c indirectly suggests that the Si migration rate is higher in case of current flow compared to purely thermal degradation (Figure 3c). This can be explained by the fact that both electron wind and thermal effects (surface diffusion can be expressed as an Arrhenius type equation) are active in the former case.

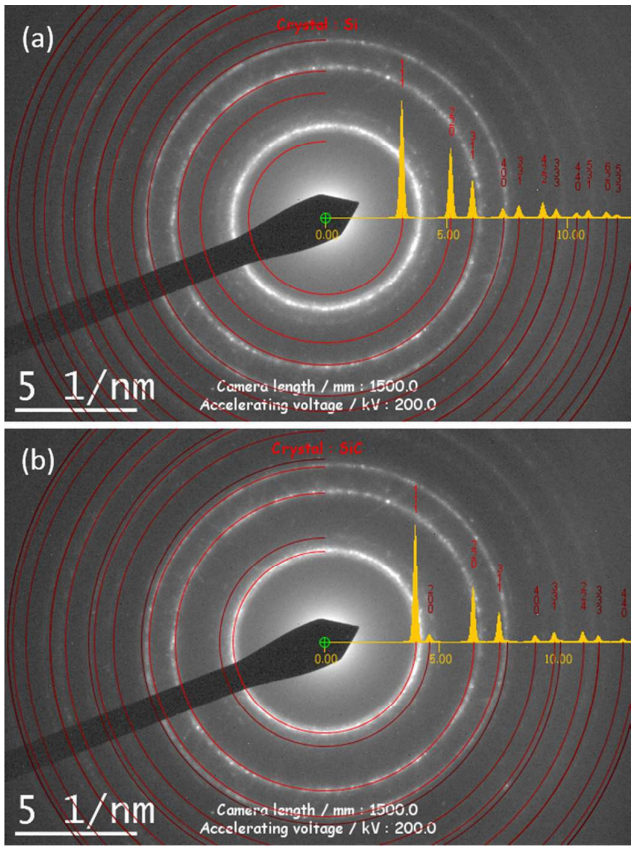

Fig. 6 TEM diffraction pattern shown in Figures 2 and 4 indexed against (a) silicon and (b) silicon carbide.

Conclusions

In this study, we experimentally investigate the structural stability and degradation of 2D WSe_2-graphene heterostructures. We developed a micro-machined test bed with heaters electrodes to apply purely thermal as well as electro-thermal fields on the directly grown freestanding heterostructure specimens. The small size of the test bed allows us to perform the experiments in-situ inside a TEM. For purely thermal loading, we found that the degradation starts with the loss of selenium at around 850 °C. This temperature is very close to that for WSe_2 deposition, which suggests remarkable stability of the heterostructure under vacuum conditions. The study also shows that the high temperature facilitates migration of foreign (contaminant) atoms, which lead to catastrophic degradation in crystallinity. For example, silicon atoms from the test-bed structure migrates to the freestanding specimen through surface diffusion. This creates instability in the crystallographic structure and it becomes very sensitive to further increase in temperature. At about 900 °C, the migrated silicon spontaneously react with the tungsten

and carbon to create nanocrystalline alloys of tungsten disilicide and silicon carbide. Under both electrical and thermal loading, the degradation process starts at temperatures 160 °C lower than thermal only loading. Even after this temperature difference, the final product is very similar, except the degraded material contains excess silicon and no carbon peaks in Raman spectra. Tungsten carbide does not form because of its very high formation temperature (around 1400 °C) for direct reaction between tungsten and carbon. In comparison, silicon reacts with carbon at 800 °C -1000 °C to form various polytypes of SiC, [36] while tungsten reacts with carbon at even lower temperatures (700 °C -900 °C) to form WSi_2.[24] Even though the present study is performed under idealized (vacuum) condition that far away from real life applications point of view, the findings inspire 2D applications under harsh environments and projects insights on degradation mechanisms. The contribution of this study is therefore to show that high temperature and current density can induce migration of foreign contaminants (silicon atoms that move from the supporting structures towards the specimen) due to phenomena similar to thermo and electromigration and alloying with foreign elements lead to catastrophic degradation in crystallinity. I.

Acknowledgements

Support is acknowledged by the Center for Low Energy Systems Technology (LEAST), one of six centers supported by the STARnet phase of the Focus Center Research Program (FCRP), a Semiconductor Research Corporation program sponsored by MARCO and DARPA.

References

1. A. C. Ferrari, F. Bonaccorso, V. Fal'ko, K. S. Novoselov, S. Roche, P. Boggild, S. Borini, F. H. L. Koppens, V. Palermo, N. Pugno, J. A. Garrido, R. Sordan, A. Bianco, L. Ballerini, M. Prato, E. Lidorikis, J. Kivioja, C. Marinelli, T. Ryhanen, A. Morpurgo, J. N. Coleman, V. Nicolosi, L. Colombo, A. Fert, M. Garcia-Hernandez, A. Bachtold, G. F. Schneider, F. Guinea, C. Dekker, M. Barbone, Z. Sun, C. Galiotis, A. N. Grigorenko, G. Konstantatos, A. Kis, M. Katsnelson, L. Vandersypen, A. Loiseau, V. Morandi, D. Neumaier, E. Treossi, V. Pellegrini, M. Polini, A. Tredicucci, G. M. Williams, B. Hee Hong, J.-H. Ahn, J. Min Kim, H. Zirath, B. J. van Wees, H. van der Zant, L. Occhipinti, A. Di Matteo, I. A. Kinloch, T. Seyller, E. Quesnel, X. Feng, K. Teo, N. Rupesinghe, P. Hakonen, S. R. T. Neil, Q. Tannock, T. Lofwander and J. Kinaret, *Nanoscale*, 2015, **7**, 4598-4810.
2. S. Z. Butler, S. M. Hollen, L. Cao, Y. Cui, J. A. Gupta, H. R. Gutiérrez, T. F. Heinz, S. S. Hong, J. Huang, A. F. Ismach, E. Johnston-Halperin, M. Kuno, V. V. Plashnitsa, R. D. Robinson, R. S. Ruoff, S. Salahuddin, J. Shan, L. Shi, M. G. Spencer, M. Terrones, W. Windl and J. E. Goldberger, *ACS Nano*, 2013, **7**, 2898-2926.
3. M. Shanmugam, R. Jacobs-Gedrim, C. Durcan and B. Yu, *Nanoscale*, 2013, **5**, 11275-11282.
4. Y. Shi, H. Li and L.-J. Li, *Chemical Society Reviews*, 2015, **44**, 2744-2756.
5. H. Wang, F. Liu, W. Fu, Z. Fang, W. Zhou and Z. Liu, *Nanoscale*, 2014, **6**, 12250-12272.
6. K. F. Mak, K. L. McGill, J. Park and P. L. McEuen, *Science*, 2014, **344**, 1489-1492.
7. K. F. Mak, C. Lee, J. Hone, J. Shan and T. F. Heinz, *Physical Review Letters*, 2010, **105**, 136805.
8. Q. H. Wang, K. Kalantar-Zadeh, A. Kis, J. N. Coleman and M. S. Strano, *Nat Nano*, 2012, **7**, 699-712.
9. D. Solenov and K. A. Velizhanin, *Physical Review Letters*, 2012, **109**, 095504.
10. S. Das, R. Gulotty, A. V. Sumant and A. Roelofs, *Nano Letters*, 2014, **14**, 2861-2866.
11. J. Huang, L. Yang, D. Liu, J. Chen, Q. Fu, Y. Xiong, F. Lin and B. Xiang, *Nanoscale*, 2015, **7**, 4193-4198.
12. S. Das and J. Appenzeller, *Applied Physics Letters*, 2013, **103**, 103501.
13. J.-K. Huang, J. Pu, C.-L. Hsu, M.-H. Chiu, Z.-Y. Juang, Y.-H. Chang, W.-H. Chang, Y. Iwasa, T. Takenobu and L.-J. Li, *ACS Nano*, 2014, **8**, 923-930.
14. N. R. Pradhan, D. Rhodes, S. Memaran, J. M. Poumirol, D. Smirnov, S. Talapatra, S. Feng, N. Perea-Lopez, A. L. Elias, M. Terrones, P. M. Ajayan and L. Balicas, *Sci. Rep.*, 2015, **5**.
15. J. I. J. Wang, Y. Yang, Y.-A. Chen, K. Watanabe, T. Taniguchi, H. O. H. Churchill and P. Jarillo-Herrero, *Nano Letters*, 2015, **15**, 1898-1903.
16. H. Fang, S. Chuang, T. C. Chang, K. Takei, T. Takahashi and A. Javey, *Nano Letters*, 2012, **12**, 3788-3792.
17. K. Jia, Y. Su, Y. Chen, J. Luo, J. Yang, P. Lv, Z. Zhang, H. Zhu, C. Zhao and T. Ye, *Vacuum*, 2015, **116**, 90-95.
18. H. Y. Nan, Z. H. Ni, J. Wang, Z. Zafar, Z. X. Shi and Y. Y. Wang, *Journal of Raman Spectroscopy*, 2013, **44**, 1018-1021.
19. X. Lu, M. I. B. Utama, J. Zhang, Y. Zhao and Q. Xiong, *Nanoscale*, 2013, **5**, 8904-8908.
20. R. K. Singh Raman, P. Chakraborty Banerjee, D. E. Lobo, H. Gullapalli, M. Sumandasa, A. Kumar, L. Choudhary, R. Tkacz, P. M. Ajayan and M. Majumder, *Carbon*, 2012, **50**, 4040-4045.
21. J. D. Wood, S. A. Wells, D. Jariwala, K.-S. Chen, E. Cho, V. K. Sangwan, X. Liu, L. J. Lauhon, T. J. Marks and M. C. Hersam, *Nano Letters*, 2014, **14**, 6964-6970.
22. S. M. Eichfeld, L. Hossain, Y.-C. Lin, A. F. Piasecki, B. Kupp, A. G. Birdwell, R. A. Burke, N. Lu, X. Peng, J. Li, A. Azcatl, S. McDonnell, R. M. Wallace, M. J. Kim, T. S. Mayer, J. M. Redwing and J. A. Robinson, *ACS Nano*, 2015, **9**, 2080-2087.
23. A. Azizi, S. Eichfeld, G. Geschwind, K. Zhang, B. Jiang, D. Mukherjee, L. Hossain, A. F. Piasecki, B. Kabius, J. A. Robinson and N. Alem, *ACS Nano*, 2015, DOI: 10.1021/acsnano.5b01677.
24. Y.-C. Lin, C.-Y. S. Chang, R. K. Ghosh, J. Li, H. Zhu, R. Addou, B. Diaconescu, T. Ohta, X. Peng, N. Lu, M. J. Kim, J. T. Robinson, R. M. Wallace, T. S. Mayer, S. Datta, L.-J. Li and J. A. Robinson, *Nano Letters*, 2014, **14**, 6936-6941.
25. A. Allain and A. Kis, *ACS Nano*, 2014, **8**, 7180-7185.
26. B. W. H. Baugher, H. O. H. Churchill, Y. Yang and P. Jarillo-Herrero, *Nat Nano*, 2014, **9**, 262-267.
27. G. Clark, S. Wu, P. Rivera, J. Finney, P. Nguyen, D. H. Cobden and X. Xu, *APL Materials*, 2014, **2**, 101101.

28. X. Kai, W. Zhenxing, D. Xiaolei, S. Muhammad, J. Chao and H. Jun, *Nanotechnology*, 2013, **24**, 465705.
29. B. Paul, E. Sarah, Z. Kehao, H. Lorraine, L. Yu-Chuan, W. Ke, L. Ning, A. R. Waite, A. A. Voevodin, K. Moon and A. R. Joshua, *2D Materials*, 2015, **2**, 014003.
30. X. Li, W. Cai, J. An, S. Kim, J. Nah, D. Yang, R. Piner, A. Velamakanni, I. Jung, E. Tutuc, S. K. Banerjee, L. Colombo and R. S. Ruoff, *Science*, 2009, **324**, 1312-1314.
31. B. Wang and M. A. Haque, *JOM*, 2015, DOI: 10.1007/s11837-015-1459-8, 1-8.
32. C. Tao, W. G. Cullen and E. D. Williams, *Science*, 2010, **328**, 736-740.
33. K. A. Velizhanin, N. Dandu and D. Solenov, *Physical Review B*, 2014, **89**, 155414.
34. J. H. Parker, D. W. Feldman and M. Ashkin, *Physical Review*, 1967, **155**, 712-714.
35. J. Huran, A. Valovič, P. Boháček, V. N. Shvetsov, A. P. Kobzev, S. B. Borzakov, A. Kleinová, M. Sekáčová, J. Arbet and V. Sasinková, *Applied Surface Science*, 2013, **269**, 88-91.
36. L. Moro, A. Paul, D. Lorents, R. Malhotra, R. Ruoff, P. Lazzeri, L. Vanzetti, A. Lui and S. Subramoney, *Journal of applied physics*, 1997, **81**, 6141-6146.